Study on Multi Stage Forging Process with Combination of Different Strain Rate and Temperature Regime in IMI 685 Forging

Jayanthi A (a_jayanthi_82@yahoo.com)
Hindustan Aeronautics Limited https://orcid.org/0000-0002-6287-821X
Anil Kumar M
Hindustan Aeronautics Ltd
Raghavendra R Bhat
Hindustan Aeronautics Ltd
Ravisankar B
National Institute of Technology Tiruchirappalli

Research Article

Keywords: IMI 685, Compressor Disc, Creep, Non-isothermal Forging, Near alpha Ti alloy, Simulation studies

Posted Date: February 25th, 2021

DOI: https://doi.org/10.21203/rs.3.rs-231930/v1

Study on Multi Stage Forging Process with Combination of Different Strain Rate and Temperature Regime in IMI 685 Forging

Jayanthi A[a]*, a_jayanthi_82@yahoo.com, +91 9738623600

M.Anil Kumar[a],ani002@gmail.com, +91 9901819002

Dr. R. Raghavendra Bhat[a], rr_bhat@yahoo.co.uk, +91 9845583002

Dr. B. Ravisankar[b], brs@nitt.edu, +91 9443578303

[a] -Foundry and Forge Division, Hindustan Aeronautics Limited, Bangalore, Karnataka, India

[b] – Department of Metallurgical and Materials Engineering, National Institute of Technology, Tiruchirappalli, Tamil Nadu, India

*- Corresponding Author

Address : Development Department, Foundry and Forge Division, Hindustan Aeronautics Limited, Bangalore-560017, Karnataka, India

Abstract

IMI 685, a near alpha Ti alloy has been used as high pressure compressor discs for aero engine application due to its high strength to weight ratio and high creep resistance. Compressor disc is a very critical component in an aero engine and manufacturing process plays an important role in obtaining the required mechanical properties. Generally due to a highly complex and critical product, its manufacturing process is not available in open literatures. Currently, isothermal forging is used and which is time consuming and not cost effective. Hence, in this paper non-isothermal approach of manufacturing compressor disc using a combination of hydraulic press and pneumatic hammer have been explored as an alternate. Simulation studies have been carried out using DEFORM 3D FEM software for the prediction of temperature distribution, strain and strain rate experienced during forging. Forging has been carried out in two stages, hydraulic press used for upsetting and hammer used for die forging in partial α-β / β temperature range and beta solutionised followed by aging. Extensive mechanical testing such as room temperature tensile test, hot tensile test, notch tensile test, creep, post creep tensile test and micro structural characterization has been performed. From the mechanical and metallurgical analysis it was found that processing in partial α-β / β temperature range resulted in higher creep strain rate with acicular / needle alpha platelets with a basket weave structure. This experiment has proven with a proper selection of thermo mechanical process parameter, required creep properties can be met with the non-isothermal processing route.

Keywords

IMI 685; Compressor Disc; Creep; Non-isothermal Forging; Near alpha Ti alloy; Simulation studies

1. Introduction

IMI 685 (Ti-6Al-5Zr-0.5Mo-0.25 Si), a near alpha Titanium alloy widely used as compressor disc material for gas turbine aircraft engines, because of its high specific strength combined with good corrosion resistance, fracture toughness, superior high temperature properties and weldability[1]. Material for compressor disc should possess sufficient strength at operating temperature (150°C -600°C) with excellent creep properties. This alloy is designed for applications up to a temperature of 520°C [2]. Thermo mechanical processing plays an important role in obtaining the required properties in IMI 685 material as mechanical properties varies with the different morphology of alpha and beta phase in the microstructure [3].

In our earlier research, methodology of using a non-isothermal forging process based on process map[4] for different operations (for low strain rate deformation, hydraulic press and for high strain rate deformation, pneumatic hammer was chosen) has been verified and proved with the help of simulation studies. The forging process parameter such as temperature and strain rate was based on the process map developed by Prasad et al.[5]. Process maps are used for the determination of processing parameters which are safe for the hot working process. The safe domains in process maps indicate the region of dynamic recrystallization and super plastic deformation which ensures microstructural control and reproducibility. Instability regions indicates mechanisms which cause microstructure damage , in-homogeneities in the microstructure caused by wedge cracking ,void formation or intercrystalline cracking or adiabatic shear bands or flow localization[4]. Based on simulation studies, experiment was carried out in entirely α-β temperature region. From the experiment, it was proved that conventional forging equipment can be used to produce IMI 685 forgings. The experiment revealed that the compressor discs forged in entirely α-β temperature region yielded higher mechanical properties such as room temperature tensile strength, notch tensile strength, post creep tensile strength and resulted in lower creep resistance (around 0.15% plastic strain against the requirement of 0.1%max at 520°C, 300 MPa for 100 hr). The microstructure revealed coarse grain (polygonal shape) of 1.2mm with standard deviation of ± 0.6mm with non-uniform distribution of grains. Based on mechanical and microstructural studies, it was understood that forging temperature and heat treatment quench delay played an important role in obtaining the higher creep resistance. This was in agreement with the established literature [3]. The manufacturing process was devised with two stages of upsetting in the hydraulic press and final die forging in the hammer to meet the requirement of process map and to avoid adiabatic heat rise resulting in non-uniform structure. In this paper, IMI 685 forgings were manufactured in α-β temperature region for the initial upsetting operation (upset stage 1) and in β temperature region for another upsetting (upset stage 2) and die forging operation (α-β / β / β processing). The forgings were beta solutionised, oil quenched with quench delay less than 30 sec in vacuum furnace followed by ageing and their mechanical and metallurgical characterization has been carried out.

Somani et al. have described about the super plastic deformation of LT26A material (which is an Indian equivalent grade of IMI 685) in the α-β temperature range (1000°C) using isothermal forming of compressor disc and compared their result with the IMI 685 disc whose manufacturing process was unknown. Mechanical properties were comparable in both the discs and creep resistance was low in LT26A disc and it was attributed to heat treatment process and the non-uniform grain size distribution (0.2 to 1mm) over the cross section of the disc[6]. Smith has provided information on the type of isothermal forging equipment used for IMI

834 disc in α-β temperature range using a single operation from billet. He has reported on the mechanical and microstructural analysis resulting from air cooling and oil quenching after solutionising treatment indicating the cooling rate also affects mechanical properties[7]. From the literature survey, it is understood; studies have been carried out using isothermal forging for IMI 685 and Ti alloys. However, information on the non-isothermal forging route was not reported widely.

In forging operation, the forging equipment also play an important role in determining the rate of deformation, temperature distribution, die chilling, etc. These factors affect the material flow behavior and the energy required to form the part. These factors can be predicted by the use of Finite Element Analysis in the virtual medium without the use of actual materials [8]. DEFORM 3D is one of the leading forging simulation software using finite element analysis that is designed to analyze the 3D flow of metal forming process. Some of the features this software can predict are temperature, strain, strain rate, velocity of metal flow, fold, non-formation, grain flow, microstructure, heat treatment response, forging load, die stress, die wear, etc [9]. In this experiment, simulation was mainly used to find out the temperature, strain, strain rate distribution, die filling, fold formation and forging load requirement.

Even though similar materials such as IMI 829 and IMI 834 have been developed after IMI 685 for the same purpose to operate on a higher temperature up to 600°C, some of the aero engines under development have chosen this material in the compressor region. Currently, many aero engines in service are designed and certified with IMI 685. Hence, there is a need to establish cost effective or better processing route to manufacture the IMI 685 forging to cater to the needs of production, repair and overhaul for existing aero engines and also to manufacture forgings for new aero engine development (e.g. some of the new engines under development also uses this material with different nomenclature).

Hence, to cater the needs of a new engine under development, old engines overhaul and reduce the cost and lead time, there is a necessity to establish the technology using non-isothermal forging route using presses and hammers to produce compressor disc. Hence, in this paper, an alternate approach by a combination of different forging equipment has been explored and the results are reported.

2. Methodology

The general steps involved in forging are upsetting to the nearest size of the forging and upset is forged in the impression dies to obtain the required grain flow.

From the process map[4], it is observed that IMI 685 material can be forged between 950°C and 1000° C with the process efficiency around 50% and strain rate from 0.001 to 0.1 per sec. The effect of temperature variation during forging will be minimum as the efficiency envelop is from 33% to 55% and there is no instability region in this envelop. Hence, this process can be accomplished by any conventional hydraulic press with appropriate insulation to reduce die chilling effect. Approximately 2000T load is sufficient for upsetting operation. An initial simulation study has been carried out with the hydraulic press for the die forging operation and found that loads are around 15000 T which is high and drop in temperature is significant due to die chilling effect. Die forging cannot be carried out in the hydraulic press due to larger load requirement and die chilling effect which results in forging at lower temperature and strain rates where it falls under the low efficiency and

instability region of process map. In view of this, hydraulic press cannot be used for die forging operation of this material. In addition to it, 15000T hydraulic press is heavy forging equipment and only few such forging presses are available in world, the option of die forging in hydraulic press is not viable. From the process map, there is another region available with higher efficiency (>40%) above 975°C and strain rate above 10 per sec. The strain rate of 10 per sec can be achieved through pneumatic or hydraulic hammers[8]. Hammer forging has a reputation as an excellent way to enhance the metallurgical properties of many materials, including high-performance materials such as waspaloy, the nickel-base superalloy used for many turbine disc applications[10]. Die chilling effect is minimum in hammer due to high operating speed, high adiabatic temperature rise inside forging and less die to part contact time compared to hydraulic press. Based on the previous experiment, ***three stages of forging have been finalized: upsetting stage 1, upsetting stage 2 in the hydraulic press and final die forging in the hammer.*** From the literature [11] it was understood that β processing can be carried out if sufficient working takes places during forging operation and β grain growth has to be controlled for better creep resistance. Hence upsetting stage 1 was decided to be carried out in α-β temperature region and upsetting stage 2 and die forging in above β transus temperature. Flow chart of the entire process is represented in Figure 1.

Based on the above information, in the present experiment, ***30MN (max) capacity of the hydraulic press is used for upsetting and pneumatic hammer which can deliver 475kJ maximum energy per blow is used for die forging operation.*** The speed of the hydraulic press is 0.01-0.0315 m/sec and for the hammer is 2.3 to 3.5 m/sec.

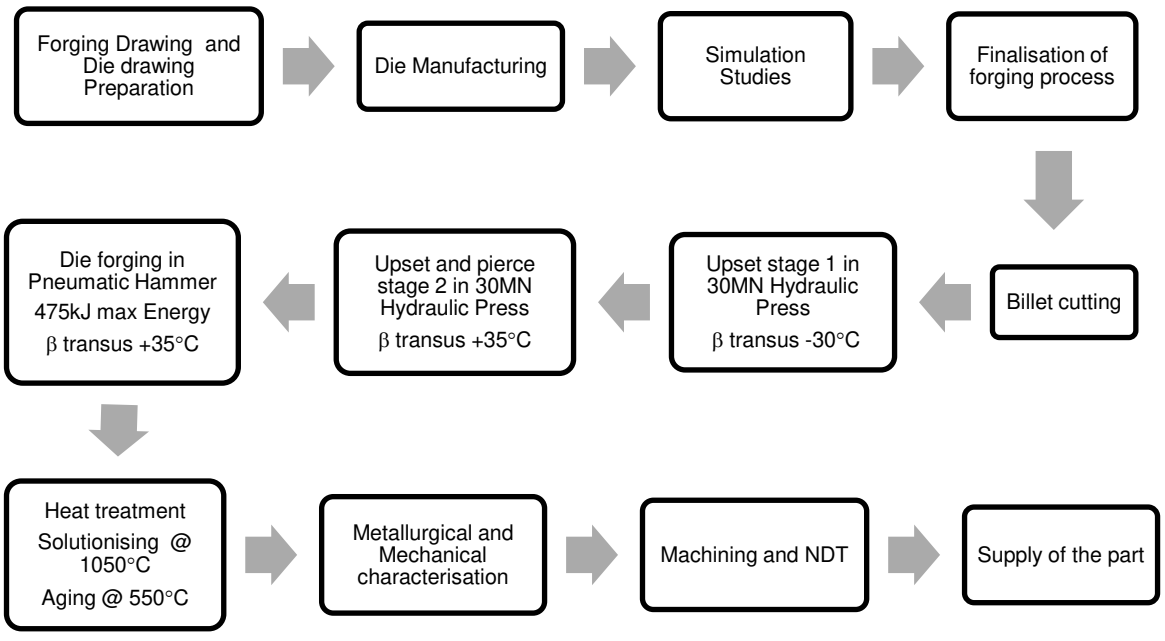

Fig. 1 Flow chart for the forging process

2.1 Design of Forging

The component drawing is the basis of forging design. Based on the component drawing, sonic profile is created to facilitate 100%volume to test internal soundness by immersion ultrasonic test. Forging drawing is prepared by adding machining allowance, draft allowance and provision for an integral test ring for testing each part for mechanical properties. The approximate size of the forging is ∅400mm x 75mm height. A combination of α-β forging for upset stage 1 and β forging for upset stage 2 and die forging has been chosen to find out the effect of temperature on the properties.

2.2 Finite Element Model and Simulation

The forging process involves different steps, namely: upsetting and die forging to form the forging profile to the required grain flow requirement. The basic details regarding the preprocessor, processor and post processor for finite element analysis is explained in literature [8]. The different process has been simulated using DEFORM 3D version 11.3 finite element software. The details regarding the pre and post processing, simulation method can be referred to DEFORM Manual. 3D CAD model of forging dies were made using UNIGRAPHICS NX10 software and exported in stereo lithographic format for the forging simulation. The boundary conditions and the material properties used for the simulation are listed in Table 1. Tetrahedral elements were used for meshing the work-piece. Co-efficient of friction was selected based on the glass lubrication of the part and the interface with a steel die block based on the data available in DEFORM 3D simulation software and verified with the other forging data available with us based on previous forging experience. Material data has been taken from the ASM handbook[11]. Other parameters were selected from the database of DEFORM 3D software.

Table 1 Boundary conditions and material parameters used in simulation

Parameters	Set Values	Material (IMI 685) Parameter	Values
Coulomb friction factor Shear friction	0.18 0.3	Elastic Modulus at Room temperature, GPa	125
Emissivity	0.7	Poisson ratio	0.36
Convection coefficient between material and atmosphere @ 25°C (N/mm/s/°C)	0.02	Specific heat capacity kJ/kgK	0.53
Heat transfer coefficient between work piece and dies during forging (N/mm/s/°C) during free resting (N/mm/s/°C)	 5 1	Beta transus (°C)	1010-1030
Transfer time of work piece from furnace and the dies(sec)	45	Thermal conductivity J/msK	4.2
Work piece resting time on dies(sec)	15	Co-efficient of thermal expansion, (x 10^{-6}mK)	101
Upsetting stage 1 in Hydraulic press	β transus-30°C	Density, g/cc	4.5
Upsetting stage 2 in Hydraulic press	β transus+35°C		
Die forging in hammer	β transus+35°C		

The following assumptions were made for simulation: (a) Upset and forging dies were rigid and die temperature as 250°C, (b) Work piece considered as plastic and set to follow an isotropic hardening flow rule and Von Mises

yielding function (c) flow stress (σ) of this material as a function of strain (ε), strain rate ($\dot{\varepsilon}$) and temperature(T) based on flow stress data from literature [5].

The top die movement for the upsetting operation is 5mm/sec in the hydraulic press. For the die forging operation, blow efficiency of 50% has been provided with 4 blows with the delay time of 1sec between the blows. Die stopping control during forging operation was set to 5 mm flash thickness. The dead zone (zone where the material is not deformed during the forging process) observed in the simulation has been removed using machining during the experiment. Accordingly, boundary conditions have been changed in simulation. The simulation was solved through conjugate gradient solver with direct iteration method. The details regarding this solver can be found in literature [9]. The simulation was analyzed for various parameters such as load requirements, formation, fold, temperature distribution, strain distribution and strain rate distribution. 12 points were chosen across the sonic profile for point tracking application to analyze the temperature, strain and strain rate. Figure 2 shows the point location used for point tracking inside the sonic profile of part along with the forging profile of compressor disc and the microstructure sample location.

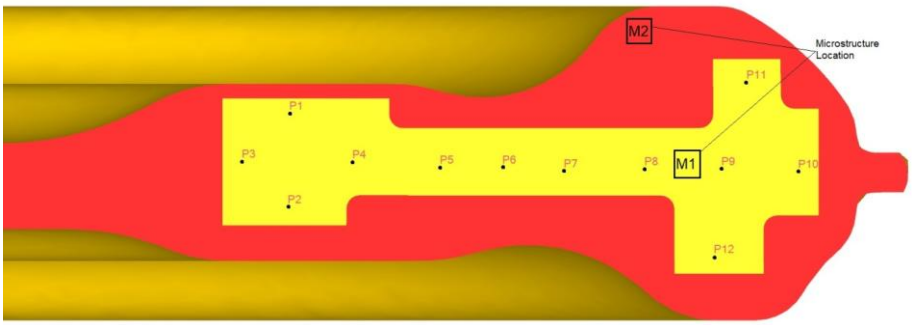

Fig. 2 Points location used for point tracking inside sonic profile within forging and microstructure location

The initial bar stock size was decided based on the final forging volume, flash width, flash thickness and dead zone material to be removed between forging operations. As this material is strain rate sensitive, dead zone is expected to be formed near die surfaces and the same has been observed in the simulation. From the simulation, dead zone height has been predicted and the extra volume required to be removed also incorporated in the bar stock dimension. The diameter has been chosen with length to diameter ratio (L/D) below 3 to avoid buckling. Accordingly, ∅150mm and 420mm length has been chosen. Detailed calculation on the bar stock finalization has been shown in Table 2.

3. Experimental Details

The material IMI 685 of ∅150 mm extruded forging bar stock was used for this study. The chemical composition is shown in Table 3.

Table 2 Bar stock size calculation

Description	Formula used	Value
Weight of part	Obtained from model	24 kg
Weight of 5mm/side of upset of size ∅345 to be removed due to fold formation (estimated using simulation)	$\Pi r^2 h\rho$ = 3.14x 172.5mm x 172.5 mm x 5mm/side x 2 sides x 4.5g/cc	4.2 kg
Slug loss of ∅100 x 40mm height due to piercing in upset stage 2	$\Pi r^2 h\rho$ =3.14 x 50mm x 50mm x 40mm x 4.5 g/cc	1.4 kg
Flash weight	10% of forging weight	2.4 kg
Total weight required	Sum of forging, material to be removed, slug loss and flash weight	32 kg
Bar stock weight	Yield of disc shape part is taken as approximately 95%	33.4 kg
Diameter chosen	Based on the length to diameter less than 3 to avoid buckling during upsetting	150 mm
Bar stock length	Weight / ($\rho\Pi r^2$) = 33400 g /(4.5 g/cc x 3.14 x 75 mm x 75 mm)	420mm

Table 3 Chemical composition (in wt %) of IMI 685 raw material

Chemical Element	**Al**	**Zr**	**Mo**	**Si**	**Fe**	**C**	**Y**
Specification requirement	5.7-6.3	4.5-6.0	0.25-0.75	0.15-0.4	0.05 max	0.08 max	10ppm max
Obtained	6.09	4.68	0.57	0.26	0.04	0.01	1
Chemical Element	**B**	**O**	**N**	**H**	**Other elements each**	**Other elements total**	**Ti**
Specification requirement	50 ppm max	0.09-0.19	0.03	100ppm max	0.1 max	0.2 max	Remainder
Obtained	1	0.14	<0.002	46	Within limit	Within limit	Remainder

Input bar stock of ∅150mm x 420 mm length rod was cut using a horizontal band saw cutting machine. The corners were smoothened to radius 10mm and top and bottom surface made flat using lathe machine. The bar stock was checked for internal soundness using contact type ultrasonic testing equipment and qualified for 1.2 mm FBH ultrasonic quality as per AMS 2630 class A1. The billets were soaked for 2hr 30 min to 3 hrs in β transus-30°C ±10 °C for upset stage 1 and β transus+35°C ±10 °C for upset stage 2 and die forging operation and dies were heated to 250°C and soaked for 5 to 6hrs in an ***electrical resistance furnace*** with tolerance of ± 14°C. (Beta transus temperature for this alloy is 1010-1020°C). Die material chosen was NCM (Nickel-Chrome-Molybdenum) die steel with hardness around 400HB (Brinell hardness number). Flat dies were used for

upsetting operation and carried out in the hydraulic press of 30MN (max) capacity. Final upset size is around ∅345 x 80 mm height (upset ratio is 5.24 after upsetting). Mica sheets were used on the die and billet interface to reduce heat loss during upsetting operation. Based on the simulation results, top and bottom surface has been removed to avoid the dead zone and chemically distorted layers. Upsets were ultrasonically checked for 1.2mm FBH (Flat Bottom Hole) for the forging uniformity through noise level study. For die forging, dies were manufactured using CNC machines to the forging profile with flash and gutter. Die forging was carried out using hammer (which can deliver 475kJ max energy per blow). Dies were soaked at 250°C and dies were loaded in press just before forging operation. As die volume is high, the decrease in die temperature was minimal and it was around 50°C during forging. Upsets were glass coated to improve lubrication and to avoid oxygen pickup before loading into the furnace. The forgings were cooled in the air after forging operation. Forged discs were pre-machined to satisfy the requirements of heat treatment (limiting section thickness for this material is 60mm[1]) and to the sonic profile. Then the forgings were β solutionised at 1050°C for 1.5 hr and Oil quenched (quench delay <30 sec) and subsequently aged at 550°C for 24 hr and air cooled.

The samples were extracted from 15 mm thick slice of the central portion of the forging using wire cutting (Figure 3a). Figure 3b shows the location of test specimen on the 15mm thick slice extracted from the forging. Tensile test at room temperature as per ASTM E8/8M, hot tensile test at 520°C as per ASTM E21, notch tensile as per ASTM E338, creep at 520°C at 300MPa for 100hrs as per ASTM E139, post creep tensile test as per ASTM E8/8M, microstructure analysis as per ASTM E3/ E407 were carried out on the specimen extracted from disc. Grain flow was analyzed as per ASTM E340. Room temperature tensile, notch tensile and hot tensile test were carried out on Tira UTM machine. Creep test carried out in 50 kN single lever arm Microtest creep testing machine. Post creep tensile test was carried out in Instron universal testing machine. The microstructure sample of raw material was taken from the center of the 10mm slice of ∅150mm diameter. Microstructure samples were polished and etched with Kroll's reagent (5%HF+ 12%HNO_3+83% H_2O) and analyzed using Leica stereo microscope. SEM analysis for alpha layer thickness was carried out using Carl Zeiss make, EVO18 Research SEM. The forgings were ultrasonically tested using immersion ultrasonic testing to 0.5mm FBH qualifying standard using 4 axis (3 axis + turn table) CNC operated immersion ultrasonic machine using 8 inch focus probes. C-scan reports were studied up to the limit of 0.5mm FBH and noise level up to 0.25mm. The results are compared with standard literature[6]. The forgings were macro etched with etchant (180-220g/l HNO_3 + 8-10g/l HF + Water balance) to find out the macro structure.

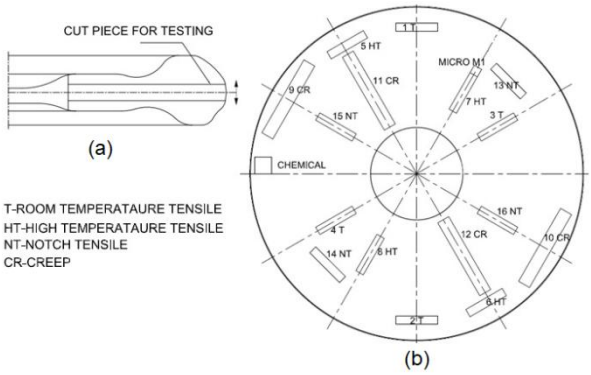

Fig. 3(a) Location of test specimen in the forging and (b) individual test specimen location on the sectioned part from forging

4. Results and Discussion

4.1 Simulation Results

Simulation results of load shows 3.2 MN required for the first upset operation and 7.2 MN for the second upset operation. Both the loads predicted suggest that with the available 30MN hydraulic press, the upset can be formed. Four blows were predicted to form part with 5mm die closure for provided hammer energy of 475kJ with 50% efficiency for each blow.

Figure 4 and Figure 5 shows the temperature and strain distribution respectively for forging after upset stage 1, 2 and die forging. From the temperature profile of upset, it is seen that top and bottom surfaces experience more heat loss compared to the centre portion due to die chilling effect. Fold is also predicted at the initial bar stock circumference due to material characteristic and die chilling effect (Figure 4b). From the temperature and strain distribution, dead zone around 5mm on the top and bottom surface (Figure 4b) has been predicted. The same height has been removed in the actual upset before the die forging operation.

Air transfer of 45 sec and 15 sec upset resting on the die has been simulated before the die forging operation. From the Figure 5, it is seen that temperature drop at the points P1, P2, P3, P10, P11, P12 was more due to their position near to surfaces and exposed to environment compared to other points. The areas surrounding these points are experiencing the temperature below beta transus temperature. Temperature raise was noticed during the die forging operation for each blow but till the completion of the die forging operation temperature raise predicted was well below the beta transus temperature. For other points, for the first and second blow the temperature predicted was above beta transus temperature and afterwards temperature dropped below beta transus temperature. This is due to dwell time in between each blow and as the part started forming, lateral movement of the material takes place and the surface area increased. As the surface area is increasing, the heat loss is more and hence the drop in temperature is observed. The forging was aimed to be carried out above beta transus temperature; however, simulation predicted the temperature during die forging will be below the beta transus temperature inside the sonic profile. The forging simulation after four blows in the hammer predicted that larger part of forging experiences temperature below beta transus. From Figure 6, it is seen than for all points, temperature after die forging has dropped below beta transus temperature (1020°C). Only a small area which is coming in contact with the top die has shown an increase in temperature and at flash region, temperature increased due to the high friction. The temperature drop was noticed at the bottom die due to the longer contact time of the part compared to the top retracting dies. The temperature drop during the upsetting stage was only on the outer surfaces and uniform temperature distribution was noticed due to larger volume compared to the surface area exposed to the environment. In die forging operation, as the flash thickness decreases, the temperature of part increases at the flash area and to reduce temperature variations, it was decided to stop the die forging operation as soon as part formed with a little flash (flash thickness around 5mm). From the superimposition of sonic profile part to the forging part and through point tracking of temperature (Figure 6), it was found that temperature distribution is uniform and part experiencing the higher variations is removed during machining. Die forging simulation was also carried out with a time interval between blows to account for the dissipation of adiabatic heat developed during the forging thereby minimizing the adiabatic temperature buildup during multi blow hammer forging. Based on the simulation results, actual trials have been carried out.

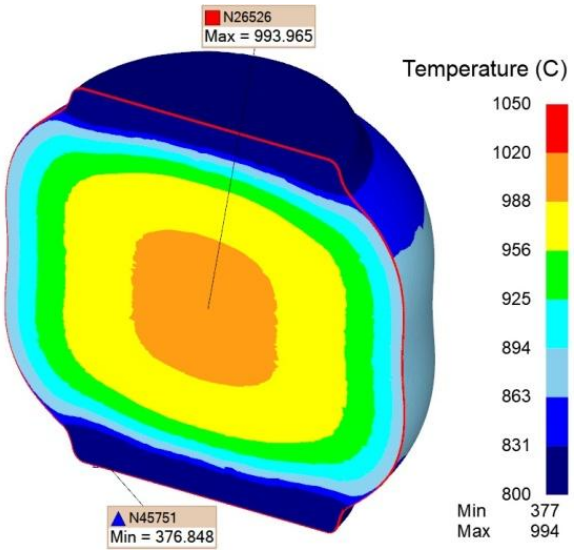

(a)

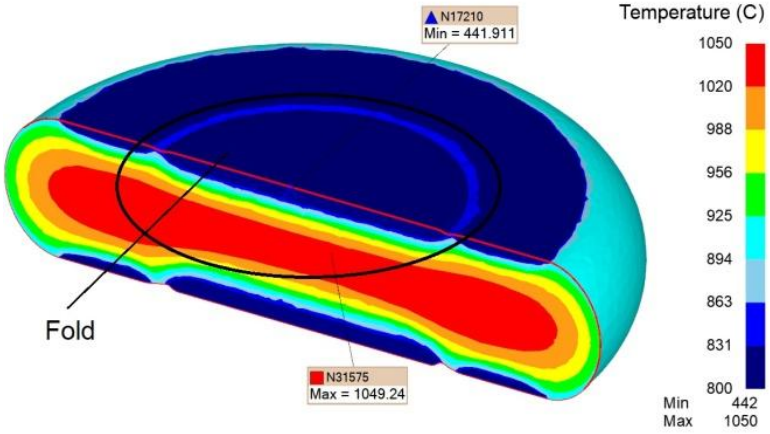

(b)

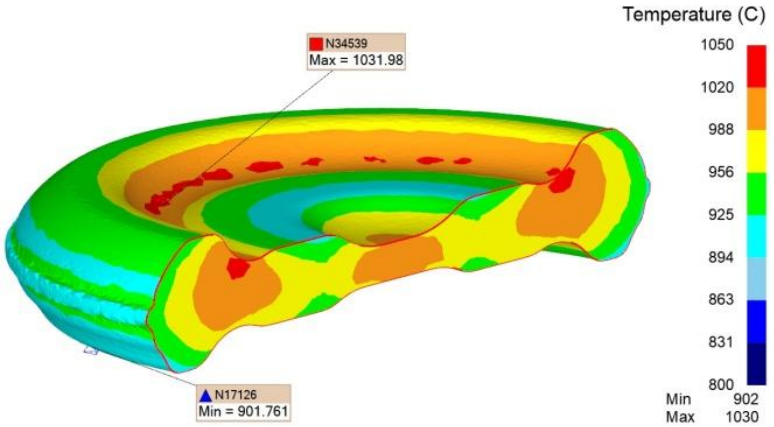

(c)

Fig. 4 Temperature distribution profile inside the disc at the end of (a) upset stage 1, (b) upset stage 2 and (c) die forging operation

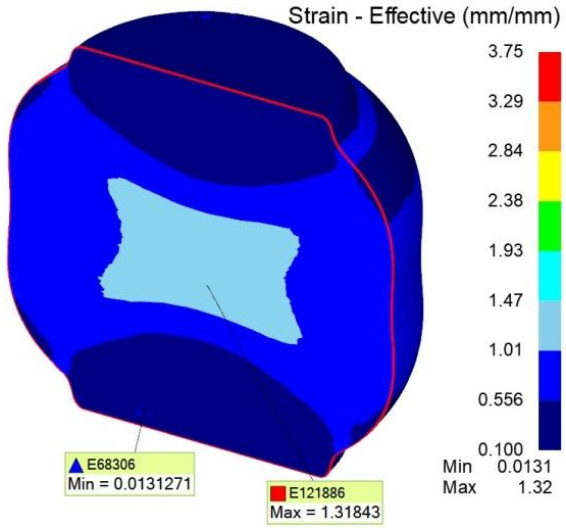

(a)

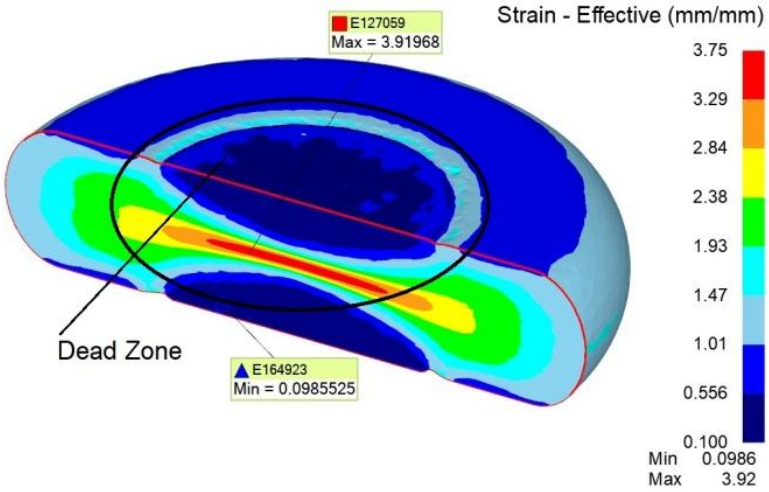

(b)

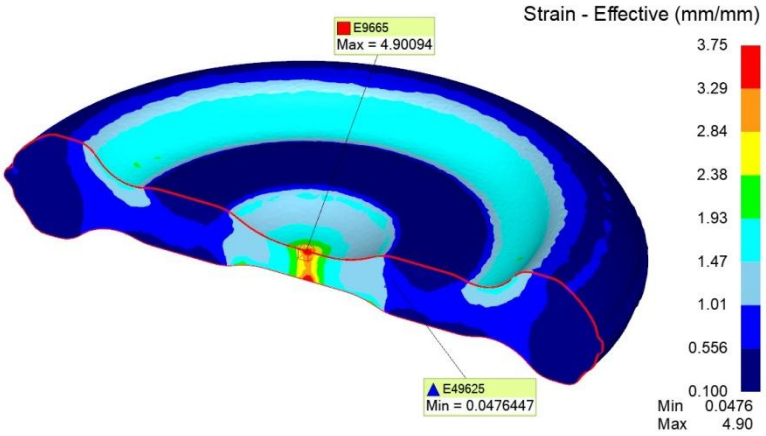

(c)

Fig. 5 Strain distribution profile inside the disc at the end of (a) upset stage 1, (b) upset stage 2 and (c) die forging operation.

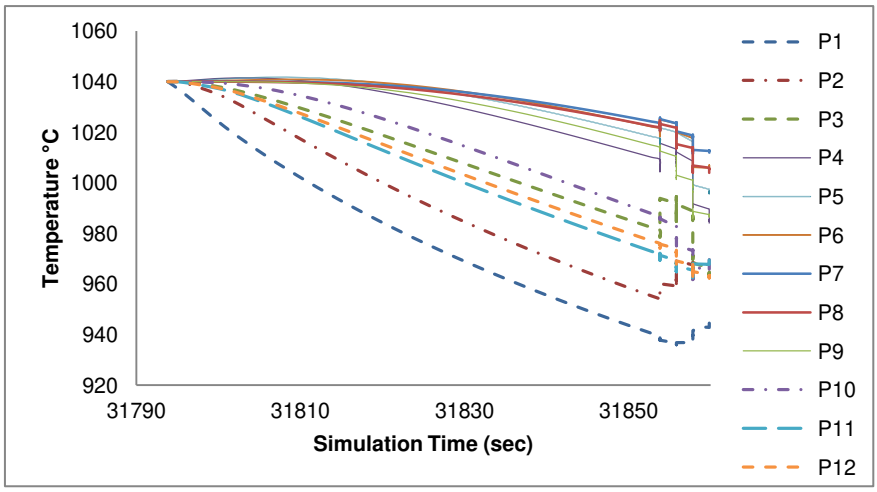

Fig. 6 Temperature distribution for points 1 to 12 during die forging

Strain rate plots for points 1 to 12 in Figure 7 shows, during upsetting stage 1 and stage 2, strain rates experienced are below 0.05 /sec and 0.12 / sec respectively for the points lying within sonic profile. The maximum strain rate experienced by the upset is 0.865 /sec which lie at the center of the forging at localized region. This region will be removed by piercing centre hole to avoid the effect of a high strain rate. Input for the final forging will have a uniform strain rate before forging. During die forging, strain rates for most of the points are less than 500/sec and it is gradually increasing for every blow of the hammer with the gradual formation of forging. At the end of the fourth blow where the full formation of part is observed with 5mm die closure, from the point tracking (Figure 8), it is seen that the maximum of 2000 /sec strain rate is experienced at point number 10 (P10) which is along the flash side. A sudden rise in strain rate is attributed to the flash formation. From the superimposition of the sonic profile, it is understood that high strain rates (>2000/sec) were experienced in the flash region and as these areas will be machined and hence, the *homogeneity of the forging* is maintained.

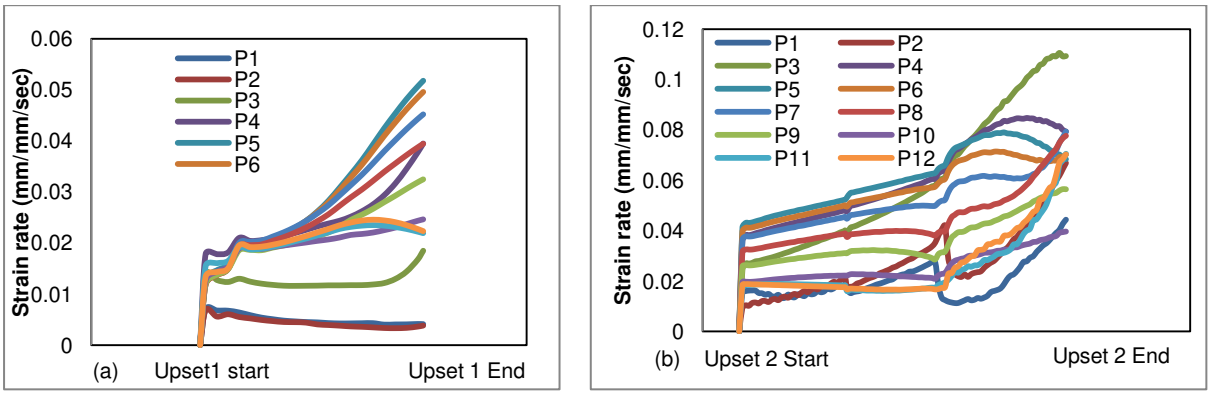

Fig. 7 Strain rate plot during (a) first stage upsetting operation and (b) second stage upsetting for point 1 to 12

In addition to it, point tracking has been carried out for 50 points all over the cross section of the forging for temperature and strain rates and an envelop has been created for determining the working domain in the process map. From envelop (Figure 9), it is understood that upsetting operation lie in the domain 2 of process map[4] and the strain rate experienced after die forging in the hammer are beyond the domain shown in

the process map. Further study on the expansion of the process map is required to understand the domains at higher strain rates.

From the simulation, it was seen that there is a gradual flow of material with a grain flow following the contour of the forging with no folding and kink formation.

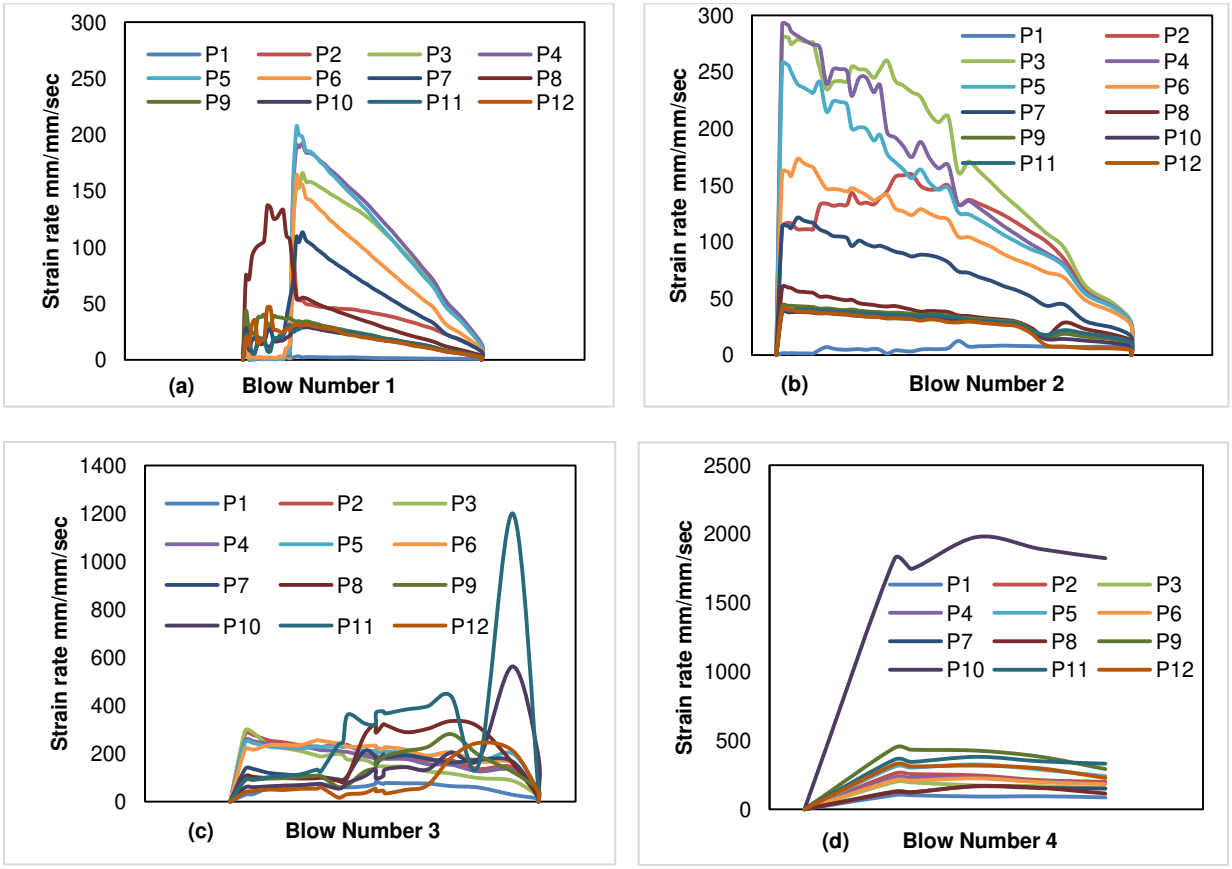

Fig. 8 Strain rate plot during die forging operation for point 1 to 12 for 4 blows

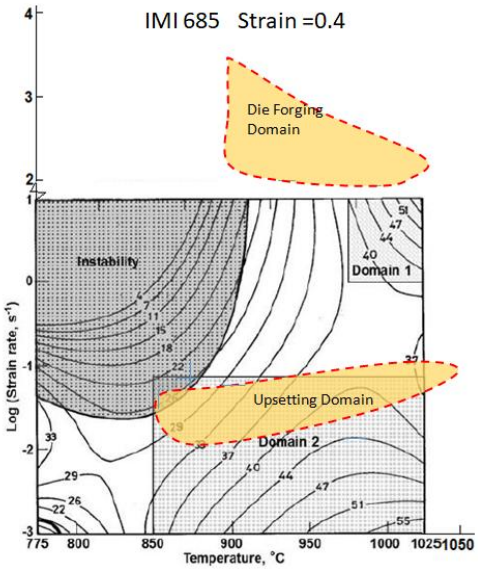

Fig. 9 Process map [4] showing the domain for present experiment

4.2 Microstructure

Figure 10 shows elongated lath primary alpha phase with fine β at the interphase boundary showing the wrought extruded structure from the sample extracted from mid radius of ∅150mm forging stock. The primary alpha lath width is 15 to 20 microns delineated with beta phase due to the presence of Mo, beta stabilizer. The base material was received in as-forged and surface machined condition which is suitable for forging operation. Figure 11 (a) and 11 (b) shows microstructure of beta solutionised and aged heat treated disc at the middle and periphery of the forging (Location of microstructure sample taken is shown in Fig. 2). It shows uniformly distributed transformed thin acicular alpha / needle alpha inside prior beta grain boundary and some areas with basket weave structure showing mixed microstructure. At the center of forging (M1), some grains show alpha needles originating at grain boundary and passing across the grains showing aligned structure. Some grains shows sub-grain structure of different orientation of alpha platelets within the same grain resulting from the different nucleation sites during cooling from solutionising treatment. At the periphery of forging, many grains shows basket weave structure which is the result of higher cooling rate compared to the centre of forging. Average grain size is 0.96mm with standard deviation of ±0.4mm. Figure 12 (a) and 12 (b) shows the SEM image of alpha layer distribution at 9600X. Individual alpha platelet thickness was less than 1.4μm at the center of forging (M1) and less than 2.2μm at the periphery (M2) indicating very fine alpha platelet has been resulted due to heat treatment. The variation in the morphology of the structure of alpha is due to the difference in the cooling rate at the surface and core of the forging. However, all the three types of alpha morphology are the result of an intermediate cooling rate resulting from the oil quenching. This indicates that sufficient cooling rate has been experienced by the part to avoid the formation of a large alpha lath which reduces the strength and creep properties[3]. From the temperature, strain and strain rate distribution analysis, uniform deformation is predicted and it is verified by the uniform grain size obtained in the forging.

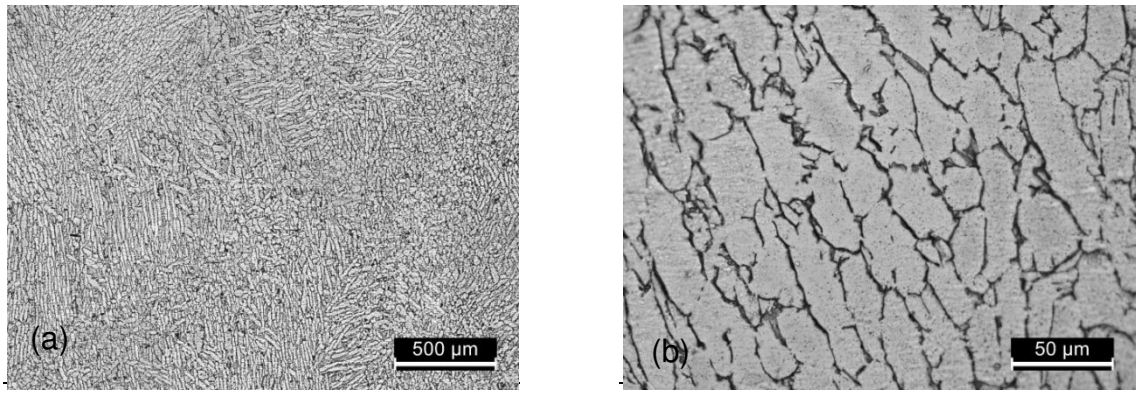

Fig. 10 Raw material microstructure showing elongated alpha grain with beta at the grain boundary (a) @50X and (b) @500X

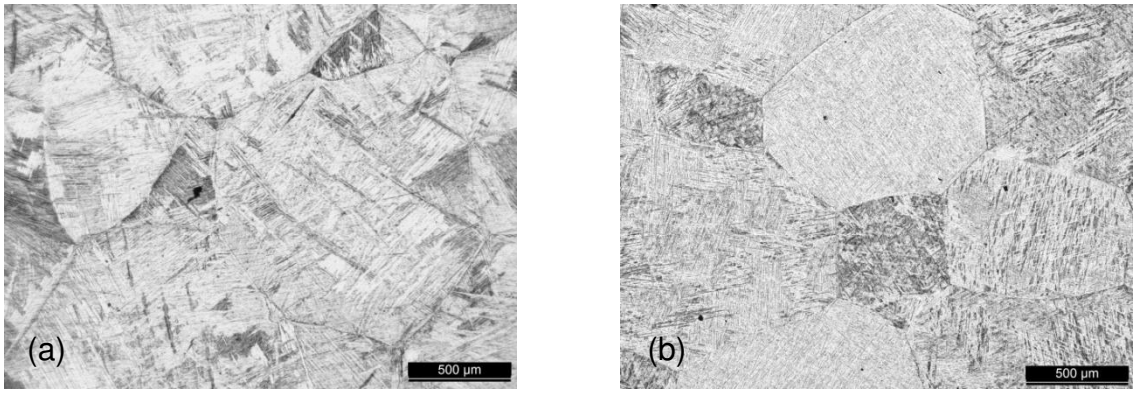

Fig. 11 Beta solutionised and aged microstructure at (a) M1 location with acicular/ needle alpha structure for the disc (50X) (@ midsection of thick section of forging) and (b) M2 location(top periphery of forging) showing acicular/needle alpha with basket weave structure

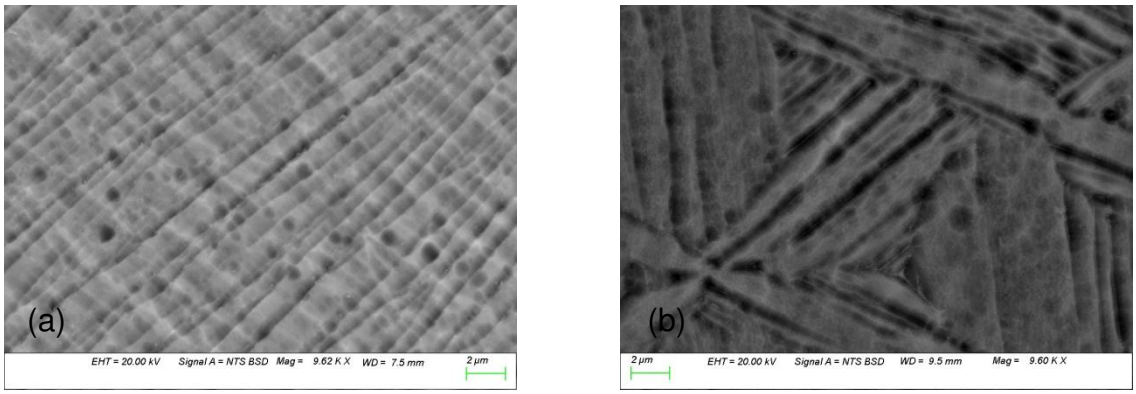

Fig. 12 SEM image @9600X showing (a) aligned alpha platelet at M1 location (midsection of thick section of forging) and (b) Basket weave structure at M2 location (top periphery of forging)

4.3 Forging characteristics

Figure 13 shows the fold formation after upsetting stage 2 at the circumference of the initial bar stock which is in line with the simulation prediction and the same has been removed by milling the top and bottom surface. Upset and die forged parts were fully formed as predicted by the simulation which indicates the chosen equipments are capable of performing the required operations. The machined upsets met the ultrasonic quality of 1.2mm FBH and noise levels were below 50% indicating the absence of non-homogeneity inside the forging. The die forged parts after machining and heat treatment were found to be ultrasonically sound below 0.5 mm FBH defect level which shows homogeneous grain distribution without any internal forging defects. Figure 14 shows the macrostructure across the cross section of forging after heat treatment and machining to sonic profile. Macrostructure examined on the machined forging surface and cross section revealed a homogenous grain structure with no heterogeneities such as alpha stabilized structures, shear bands, internal cracks and segregations. The different strain rates experienced during die forging (less than 500/sec) within the sonic profile has resulted in uniform macrostructure which indicates for this large forging, the strain rates predicted does not cause any in-homogeneities within the sonic profile. Macrostructure examination and ultrasonic inspection has confirmed that present processing conditions using non-isothermal processing using a

combination of hydraulic press and hammer has resulted in uniform structure throughout the sonic profile of forging. Grain flow (directional orientation of grains that have been deformed by forging) or flow line analysis revealed grains followed the general contour of the forging without any kinks or fold.

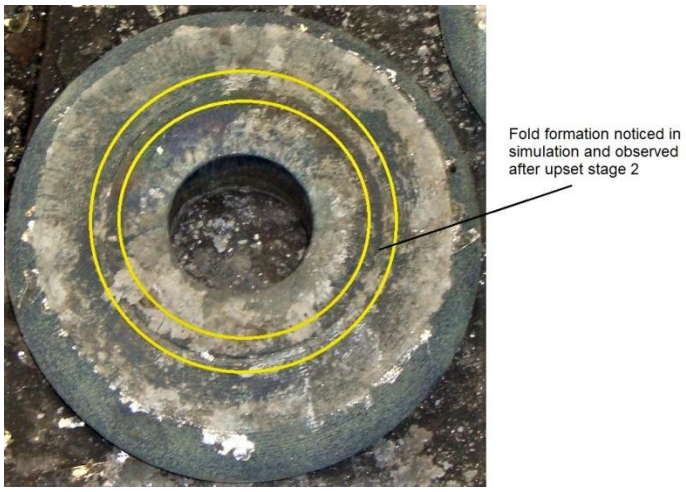

Fig. 13 The region between yellow lines indicates the fold formation observed after upsetting and piercing stage 2

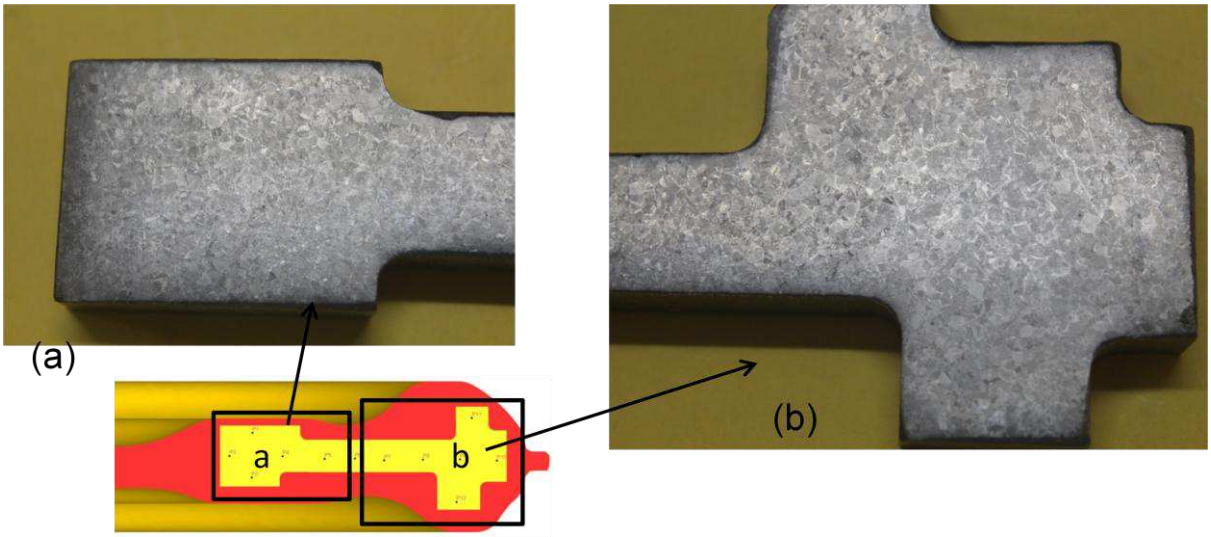

Fig. 14 Macrostructure of cross section of the forging after heat treatment and machining showing homogeneous grain distribution within the sonic profile

4.4 Mechanical properties

Table 4 shows the mechanical properties obtained for the experiment along with the literature values for the IMI 685 disc and LT26A isothermally forged disc.

Table 4: Mechanical Properties

Properties	Experiment				IMI685 Disc[6]	LT26A Disc[6]
	Tangential		Radial			
Tensile Properties at Room Temperature	1T	2T	3T	4T	Reported from literature[6]	
0.2% P.S.(MPa)	910	890	873	867	910	959
Tensile Strength (MPa)	1014	1005	973	982	1027	1034
Elongation (%)	8	10	8	8	11	9
Reduction in Area (%)	20	25	20	20	21	16
Hot Tensile properties at 520°C	5HT	6HT	7HT	8HT		
0.2% P.S.(MPa)	493	488	490	495	530	534
Tensile Strength (MPa)	612	593	623	600	681	677
Elongation (%)	15	13.5	13	11	18	16
Reduction in Area (%)	30	28	28	25	49	43
Creep Test	9CR	10CR	11CR	12CR		
Creep strain (%) at 520°C, 100hr, 300 MPa for experiment and 310MPa for IMI 685 and LT26A disc	0.054	0.071	0.097	0.064	0.04 0.05 0.02	0.10 0.14 0.10
Post Creep Tensile Properties at Room Temperature	9CR	10CR	11CR	12CR		
0.2% P.S.(MPa)	957	955	1009	918	951	996
Tensile Strength (MPa)	1015	1004	1020	969	1017	1043
Elongation (%)	8.5	6.5	5.0	9.5	11	7
Reduction in Area (%)	13	15	13	31	19	12
Notch Tensile Test at Room Temperature	13NT	14NT	15NT	16NT		
Notch Tensile Strength (MPa)	1621	1768	1775	1780	1649	1572
Notch to Plain ratio	1.6	1.76	1.82	1.81	1.61	1.52

4.4.1 Tensile test

From the Table 4, it is seen that yield strength and ultimate tensile strength for room temperature and high temperature tensile test at radial and transverse directions are comparable within the forging and comparable with an isothermally forged LT26A disc and IMI 685 disc reported in literature [6]. The mechanical properties are related to the morphology of the alpha and beta phase present in this alloy. As smaller prior β grain size improves the ductility [12], due to slightly coarse grains compared to the reported values [6], the lower elongation has resulted in the tensile test. However, the percentage RA is similar to the imported disc. Barbier et al.,[12] have reported that there is no significant variation in the mechanical properties when the part is forged in a different temperature regime. The same is observed with the experiment and the reported values[6]. From Table 4, it is seen that U.T.S. value of notch tensile test of experimental disc is approximately 100 MPa higher than the imported and isothermally forged disc[6]. Notch to plain tensile values are higher compared to published results. Higher notch tensile strength is the result of blunting of crack and change in crack orientation due to alternate alpha and beta phases aided by a thin alpha layer (less than 2.2 μm). Guo and Baker[3] have showed that beta layers between the alpha platelets are very effective in blunting the crack growth. This will improve the fracture toughness and fatigue crack propagation resistance. The same has been noticed in the present experiment.

3.4.2 Creep Test and Post Creep Room Temperature Tensile test

Figure 15 shows typical elongation versus time plot generated during the creep testing. From the figure it is observed after the instantaneous elongation, the creep curve falls under a steady state creep region till the completion of 100 hrs test duration.

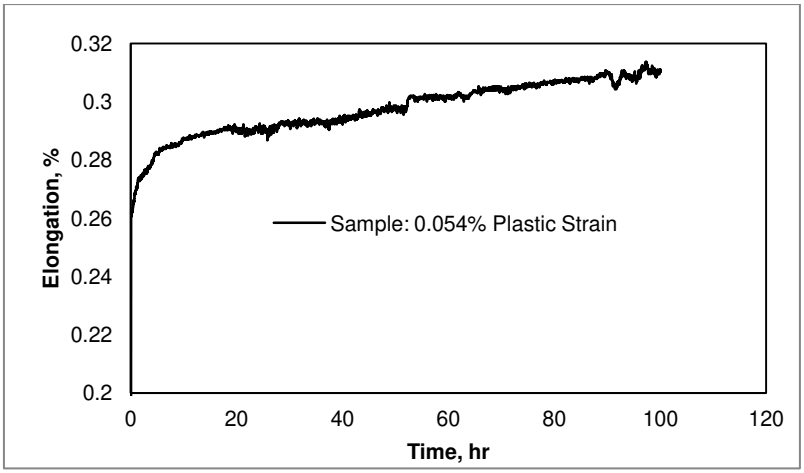

Fig. 15: Elongation versus time graph generated during creep testing

% plastic strain obtained (Table 4) is similar to literature IMI 685 disc and lesser than isothermally forged LT26A disc (Test condition: 520°C, 310 MPa stress, 100hr duration [6]. The stress is slightly higher than the present experiment. Comparison is done for reference only). From the literature [11], it is understood that the % plastic strain can be achieved less than 0.1% with the proper combination of forging and heat treatment parameters and with a prior beta grain size of 0.5-2mm. In the present experiment, grain size of 0.96 ± 0.4mm

with fine alpha platelet of less than 2.2μm, along with needle and basket weave morphology has yielded the higher creep resistance. The finer grain size and thin alpha platelet are the result of fast quenching i.e., less than 30 sec quench delay. Earlier experiment has showed thick alpha platelets which were the result of longer quench delay (more than 30 sec) and non-uniform grain size distribution which were the result of processing in entirely α-β temperature region. It is observed that beta processing is necessary for obtaining higher creep resistance and quench delay less than 30 sec also important in obtaining the mixed microstructure (basket weave and needle alpha platelet). This is in agreement with Barbier et al. [12] where they report that mixed microstructure is essential for best creep resistance. Creep resistance increases with the decrease in α platelet thickness and with an increase in discontinuous interplatelet β phase in the grain boundary[3]. Higher magnification microstructure analysis has shown the beta phase is discontinuous within the grain boundary. Isothermally forged disc shown low creep resistance and it was reported due to the heat treatment issue[6]. This indicates that the cooling rate also has influence on morphology of microstructure [11].

Post creep tensile values in Table 4 indicate that the mechanical properties of the experiment are similar to the reported IMI 685 and LT26A discs. From this experiment, it is understood that with the proper combination of forging and heat treatment process parameters, it is possible to manufacture the compressor disc through non-isothermal processing.

4. Conclusion:

A non-isothermal processing employing the combination of hydraulic press and pneumatic hammer has been studied with the manufacture of IMI 685 forging thermo mechanically processed partially in α-β and β temperature region. The combination of β working and quench delay less than 30 sec is required to yield better creep resistance which results in proper thermo mechanical working and heat treatment. Uniform grain size distribution of 0.96 ± 0.4 μm (due to forging) with acicular/ needle alpha layer having individual alpha layer thickness less than 2.2μm (result of heat treatment) has resulted in creep plastic strain less than 0.1% for 300 MPa load at 520°C for 100hrs.

From the obtained results and with the comparison of available data, it is evident that the proposed ***method of manufacturing IMI 685 forgings by a combination of hydraulic presses and hammers instead of isothermal forging can fetch the desired properties*** by controlling the process parameters as below:

- strain rate of 0.01 sec^{-1} to 0.1 sec^{-1} for upsetting operation stage 1 in β-30°C and β+35°C for upsetting operation stage 2
- strain rate of 100 sec^{-1} to 1000 sec^{-1} within the sonic profile area for the finish die forging operation in β+35°C
- removal of dead zones by machining in between operations identified through simulation.

Acknowledgement

Authors thank Mr. M.S. Venkatesh, Executive Director (Foundry and Forge Division), Hindustan Aeronautics Limited for providing all the necessary support and granting permission to publish this paper. Mr. Jaganath and Mr. Ranganath B are also being acknowledged for their support during the entire project.

Funding

This study was funded by Foundry and Forge Division, Hindustan Aeronautics Limited, Bangalore, India.

Data availability

The required Data has been provided in the paper.

Conflicts of Interest / Competing Interests

The authors have no conflicts of interest to declare that are relevant to the content of this article

Author Agreement Statement

We declare that this manuscript is original, has not been published before and is not currently being considered for publication elsewhere.

We confirm that the manuscript has been read and approved by all named authors and that there are no other persons who satisfied the criteria for authorship but are not listed.

We further confirm that the order of authors listed in the manuscript has been approved by all of us.

We understand that the Corresponding Author is the sole contact for the Editorial process. She is responsible for communicating with the other authors about progress, submissions of revisions and final approval of proofs.

Credit Author Statement

Jayanthi A : Conceptualization, Methodology, Investigation, Formal analysis and Writing - Original Draft

M.Anil Kumar : Conceptualization, Methodology, Formal analysis and Writing - Review & Editing

Dr. R. Raghavendra Bhat : Resources , Supervision, Writing - Review & Editing

Dr. B. Ravisankar : Supervision, Writing - Review & Editing

References:

1. Blenkinsop, P. A., Neal DF, Goosey RE (1982) Effect of Heat Treatment on the Microstructure and Properties of IMI 685. Titan Titan Alloy Proc 3rd Int Conf Titan 2003–2014

2. Rao N (2011) Materials for Gas Turbines – An Overview. Adv Gas Turbine Technol. https://doi.org/10.5772/20730

3. Guo ZX, Baker TN (1992) On the microstructure and thermomechanical processing of titanium alloy IMI685. Mater Sci Eng A 156:63–76. https://doi.org/10.1016/0921-5093(92)90416-X

4. Prasad YVRK, Rao KP, Sasidhara S (2015) Hot Working Guide

5. Krishna VG, Prasad YVRK, Birla NC, Rao GS (1997) Processing map for the hot working of near-α titanium alloy 685. J Mater Process Technol 71:377–383. https://doi.org/10.1016/S0924-0136(97)00102-7

6. Somani MC, Sundaresan R, Kaibyshev OA, Ermatchenko AG (1998) Deformation processing in superplasticity regime-production of aircraft engine compressor discs out of titanium alloys. Mater Sci Eng A 243:134–139. https://doi.org/10.1016/s0921-5093(97)00790-9

7. Smith DJ (1988) Isothermal forging of ti alloy-1988_Vol.3-1-Y-The_Isotherma.pdf. In: Sixth World Conference on Titanium, France. pp 1277–1281

8. Altan T, Ngaile G, Shen G (2005) Cold and Hot Forging Fundamentals and Applications

9. Specifications P (2020) DEFORM-3D. In: Sci. Form. Technol. Corp. https://www.deform.com/wp-content/uploads/2017/09/DEFORM-3D.pdf. Accessed 5 Aug 2020

10. Altan T, Shirgaokar M (2018) Selection of Forging Equipment. Metalwork Bulk Form 36–46. https://doi.org/10.31399/asm.hb.v14a.a0003974

11. Boyer R, Welsch G, Collings EW (1993) Materials Properties Handbook: Titanium Alloys. ASM International

12. Barbier F, Quesne C, Servant C (1981) Relationship between the Microstructure and the Mechanical Characteristics of Tension and Creep of the Titanium Ti 685 Alloy: Influence of the Cooling Speed and the Different Forging Conditions. J Less-Common Met 79:75–95

Figures

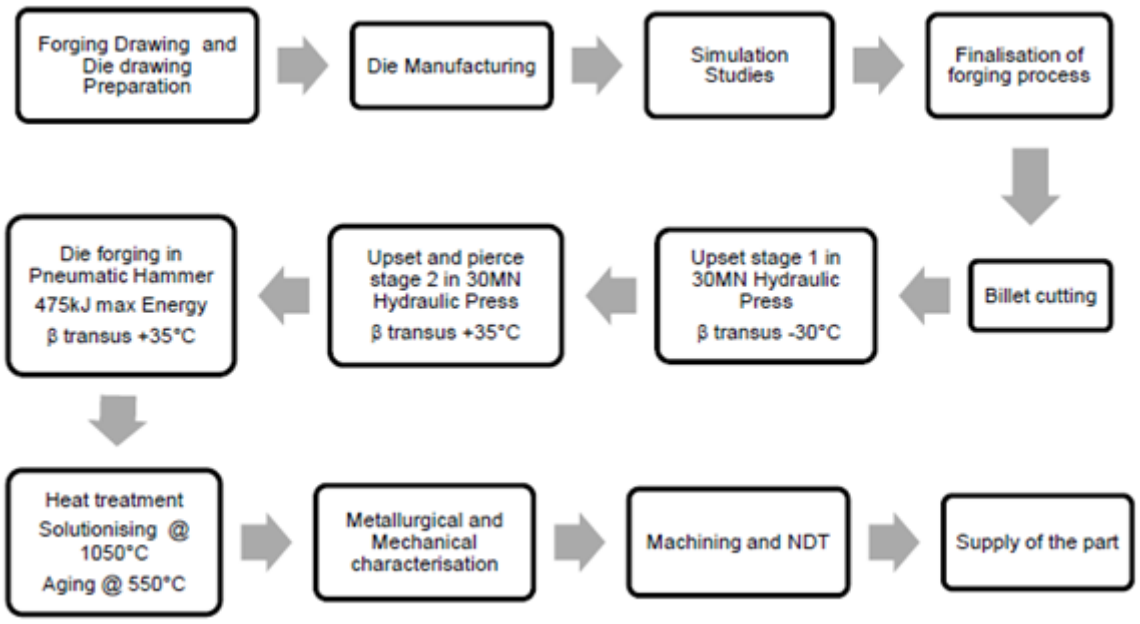

Figure 1

Flow chart for the forging process

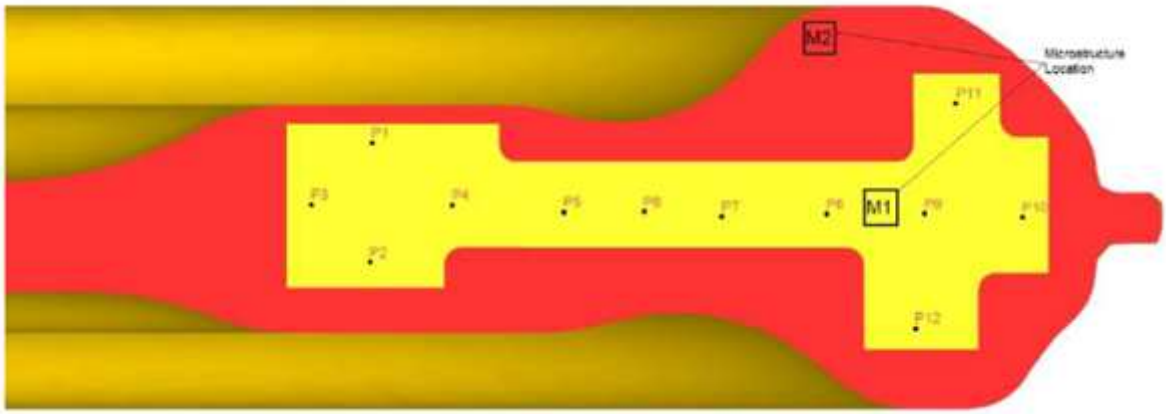

Figure 2

Points location used for point tracking inside sonic profile within forging and microstructure location

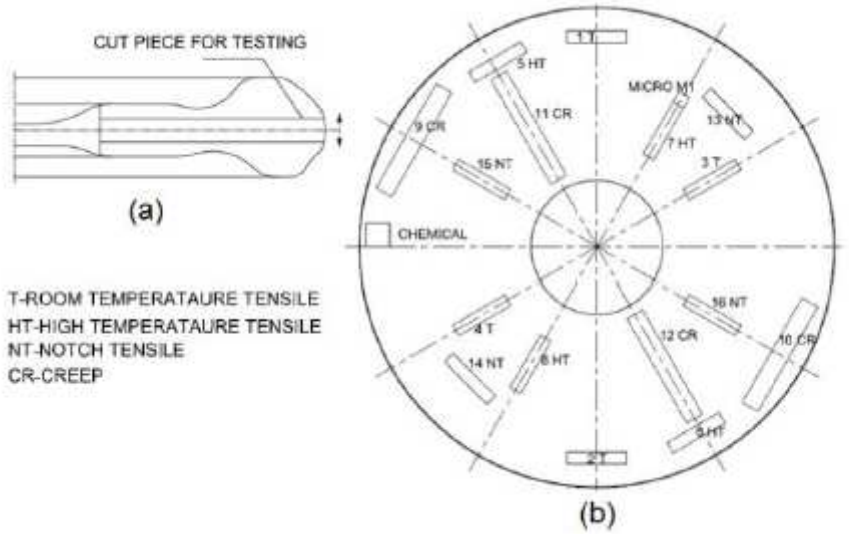

Figure 3

(a) Location of test specimen in the forging and (b) individual test specimen location on the sectioned part from forging

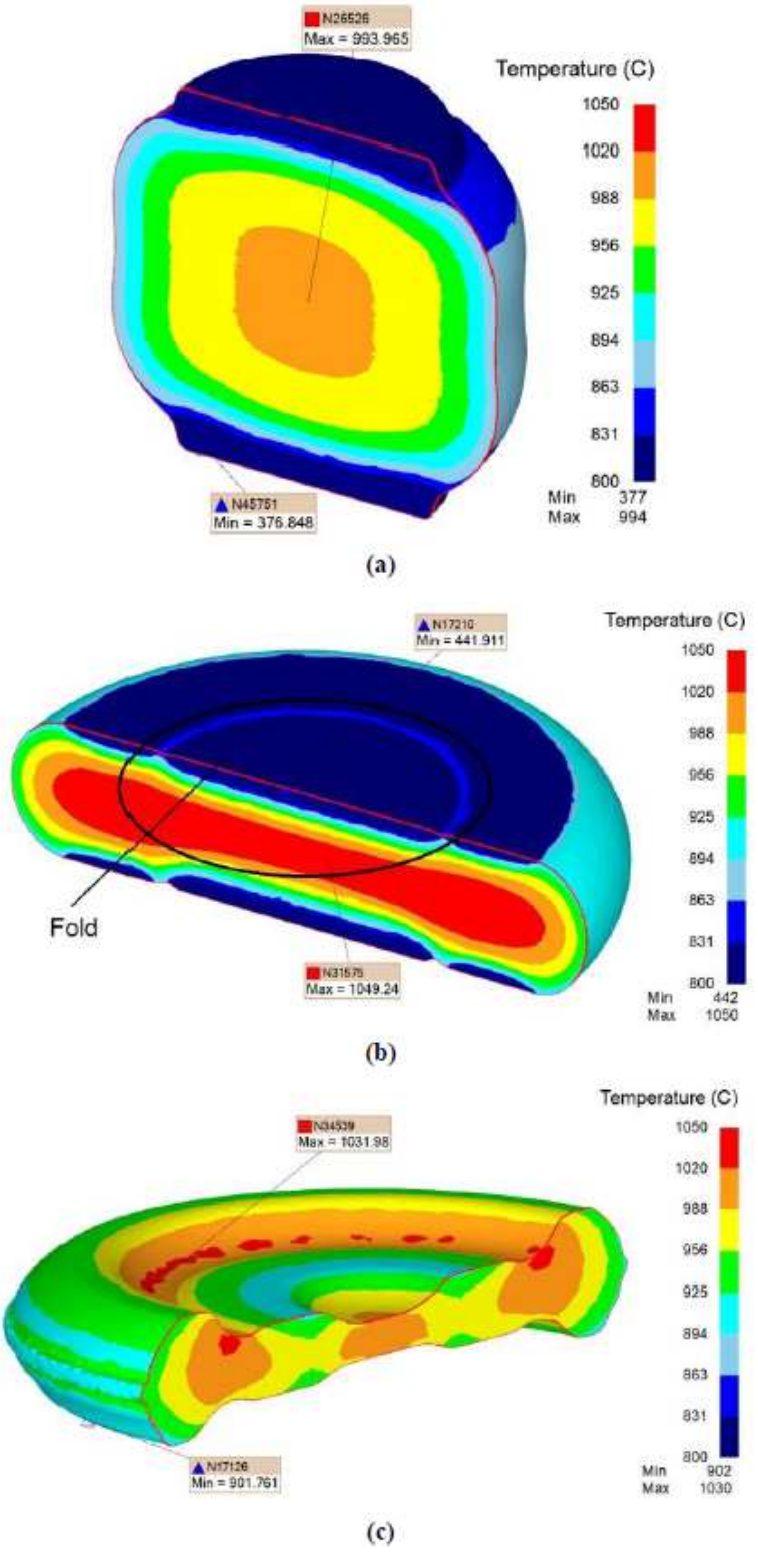

Figure 4

Temperature distribution profile inside the disc at the end of (a) upset stage 1, (b) upset stage 2 and (c) die forging operation

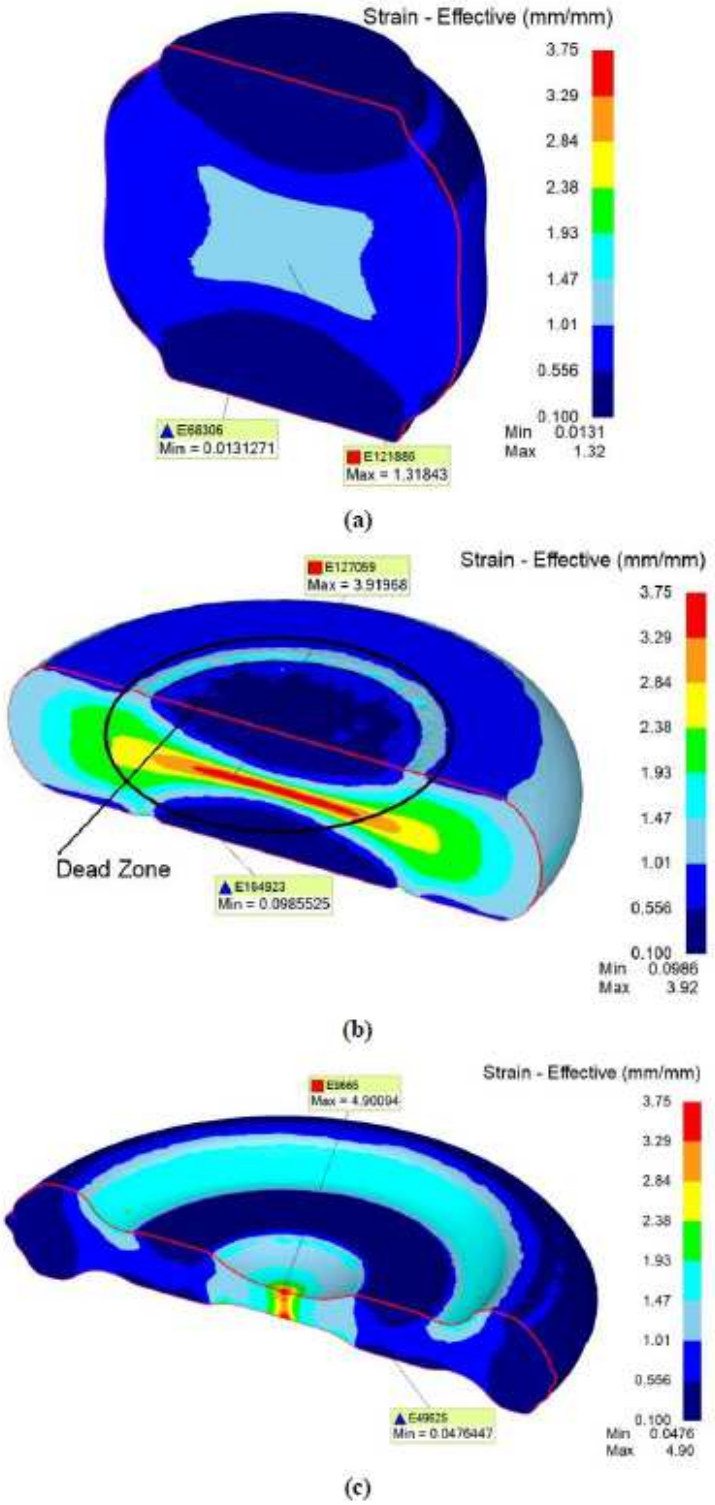

Figure 5

Strain distribution profile inside the disc at the end of (a) upset stage 1, (b) upset stage 2 and (c) die forging operation.

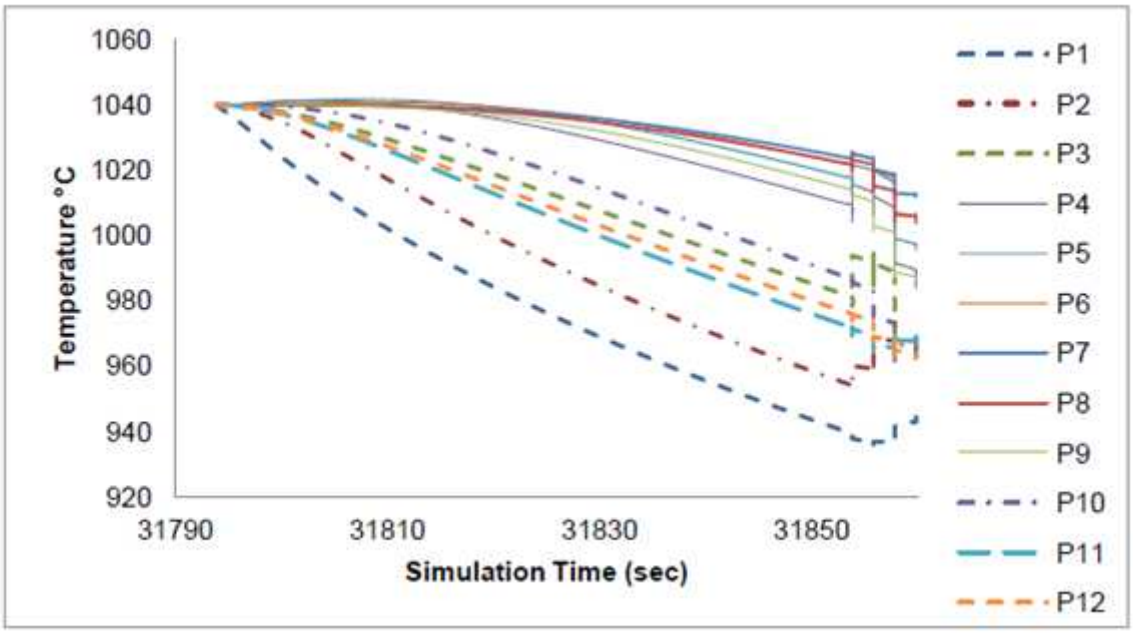

Figure 6

Temperature distribution for points 1 to 12 during die forging

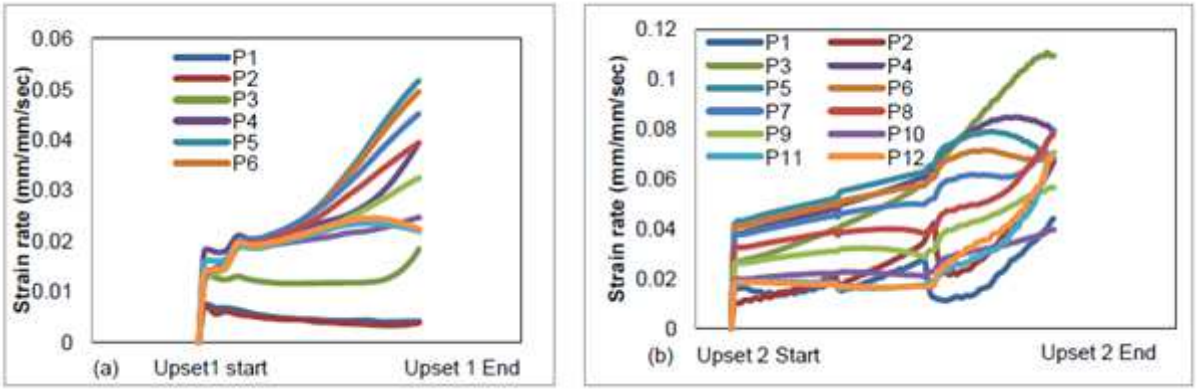

Figure 7

Strain rate plot during (a) first stage upsetting operation and (b) second stage upsetting for point 1 to 12

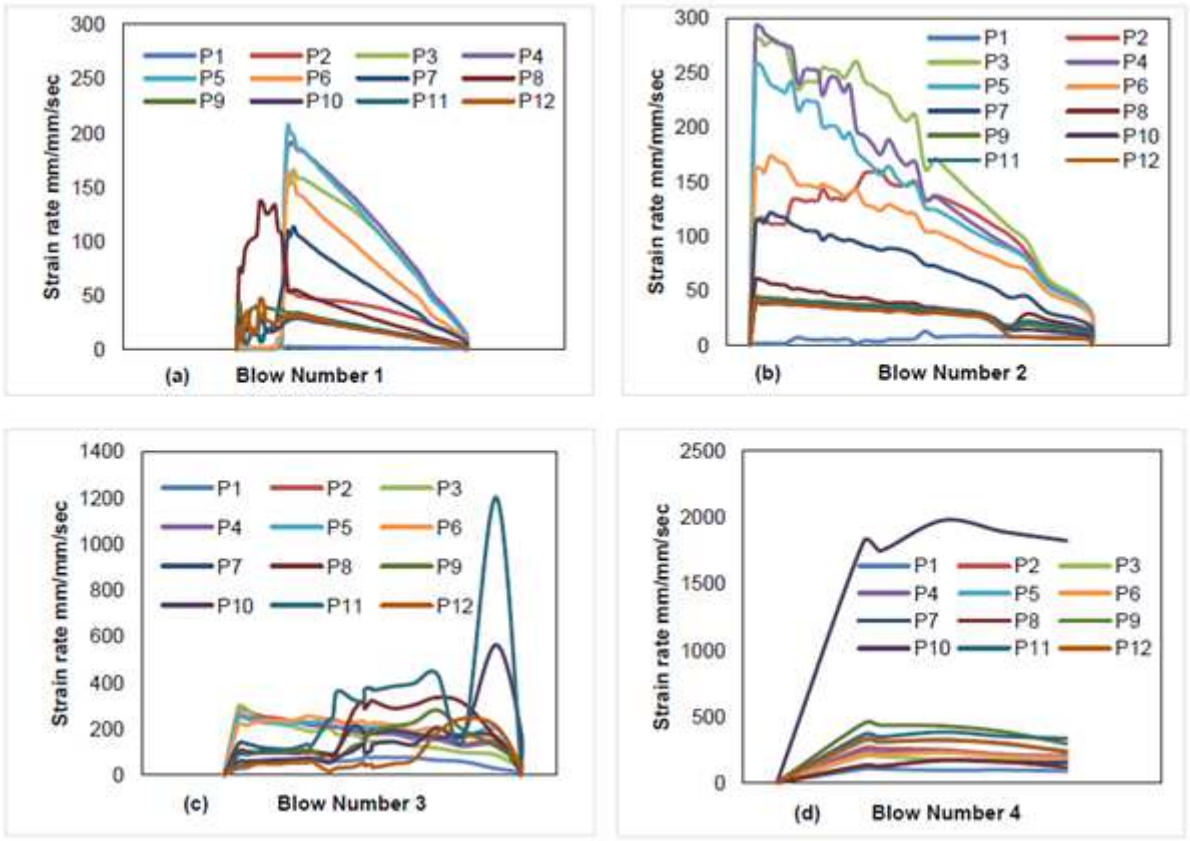

Figure 8

Strain rate plot during die forging operation for point 1 to 12 for 4 blows

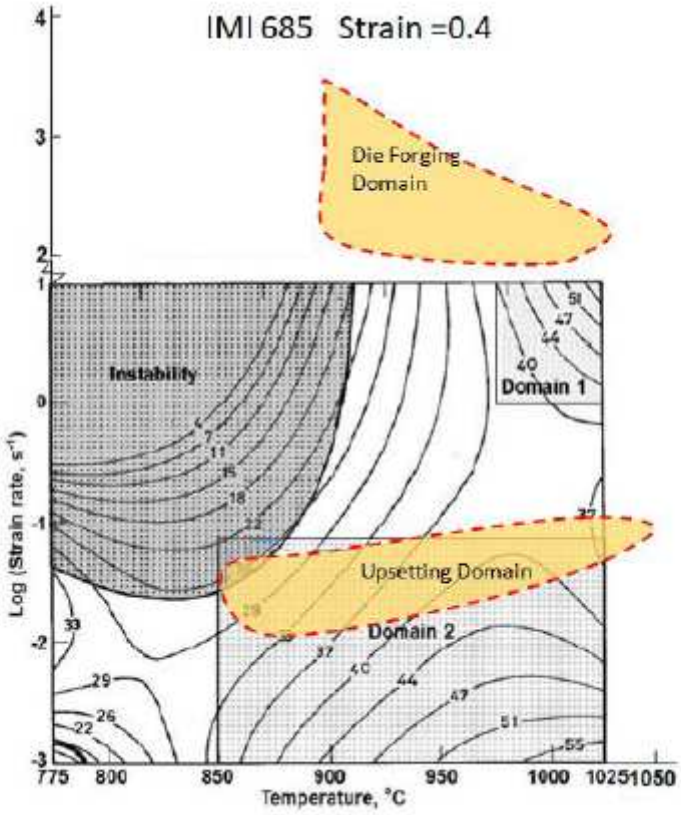

Figure 9

Process map [4] showing the domain for present experiment

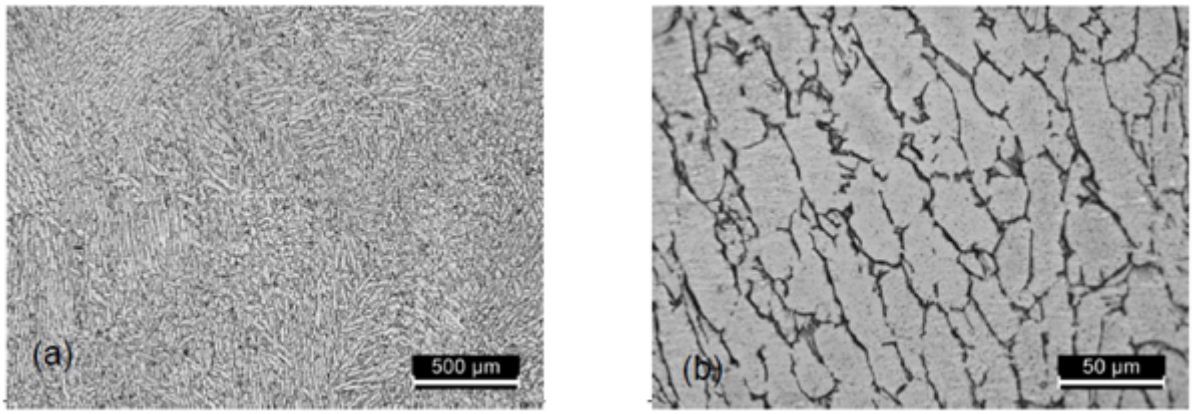

Figure 10

Raw material microstructure showing elongated alpha grain with beta at the grain boundary (a) @50X and (b) @500X

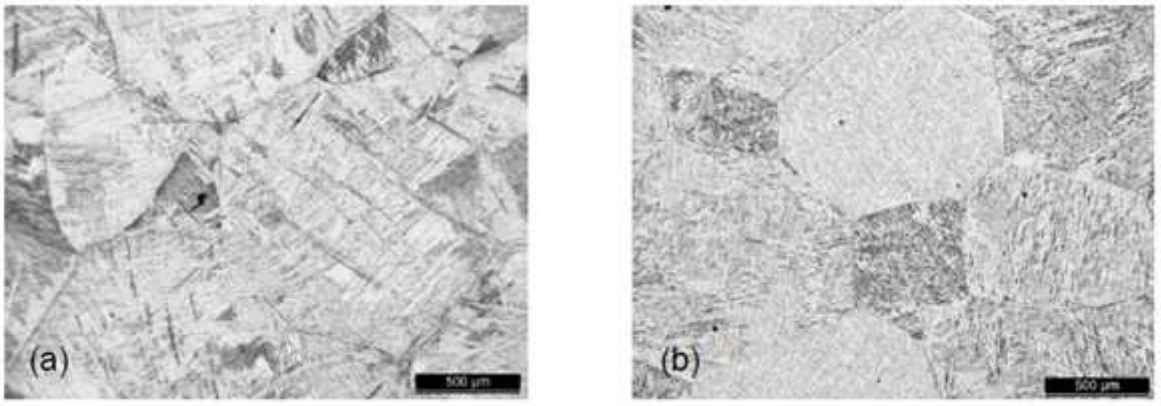

Figure 11

Beta solutionised and aged microstructure at (a) M1 location with acicular/ needle alpha structure for the disc (50X) (@ midsection of thick section of forging) and (b) M2 location(top periphery of forging) showing acicular/needle alpha with basket weave structure

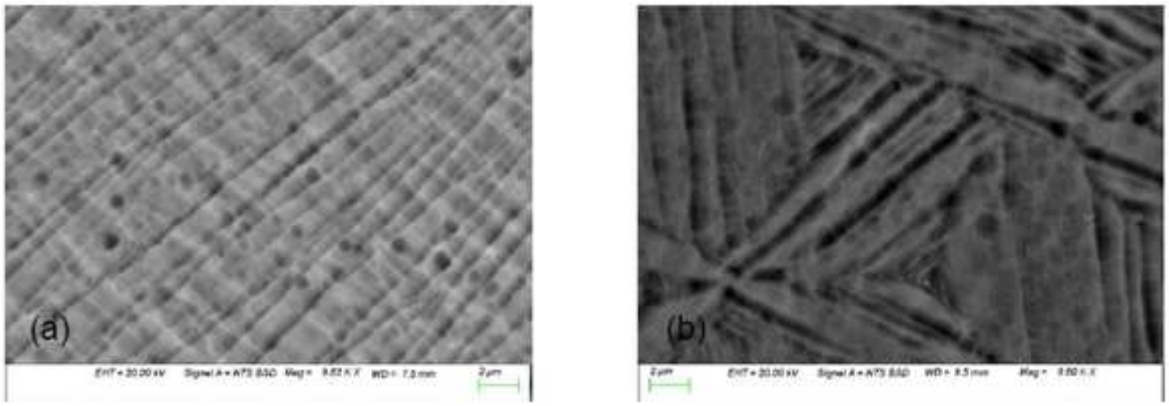

Figure 12

SEM image @9600X showing (a) aligned alpha platelet at M1 location (midsection of thick section of forging) and (b) Basket weave structure at M2 location (top periphery of forging)

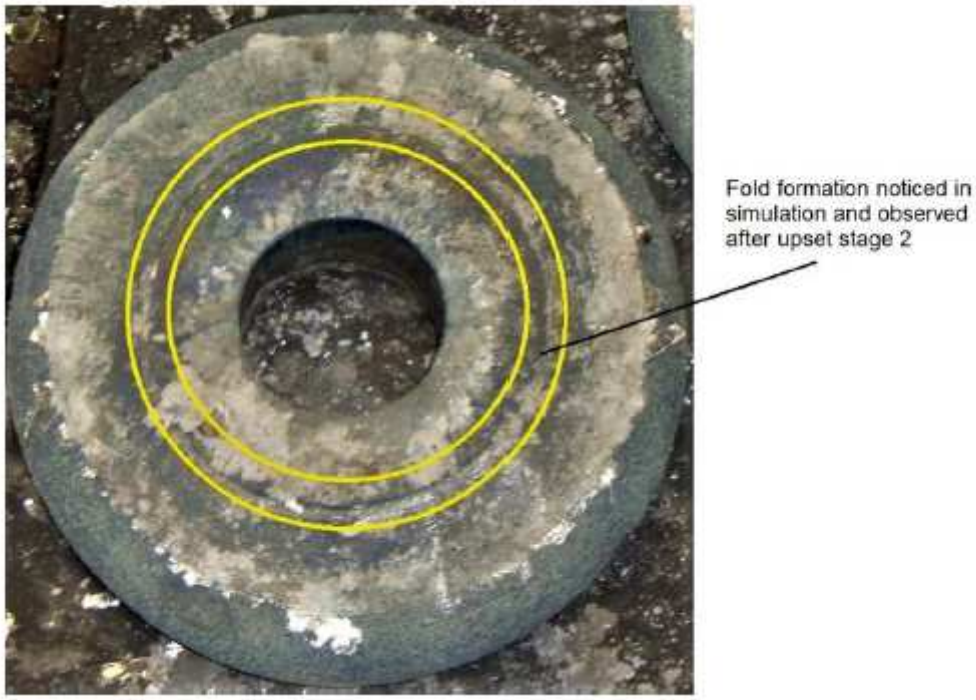

Figure 13

The region between yellow lines indicates the fold formation observed after upsetting and piercing stage 2

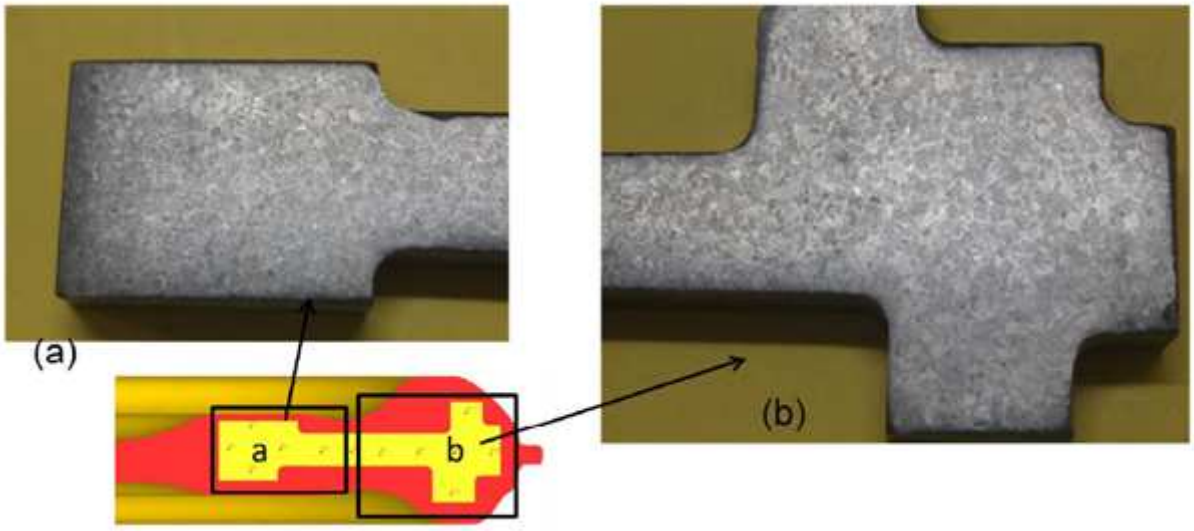

Figure 14

Macrostructure of cross section of the forging after heat treatment and machining showing homogeneous grain distribution within the sonic profile

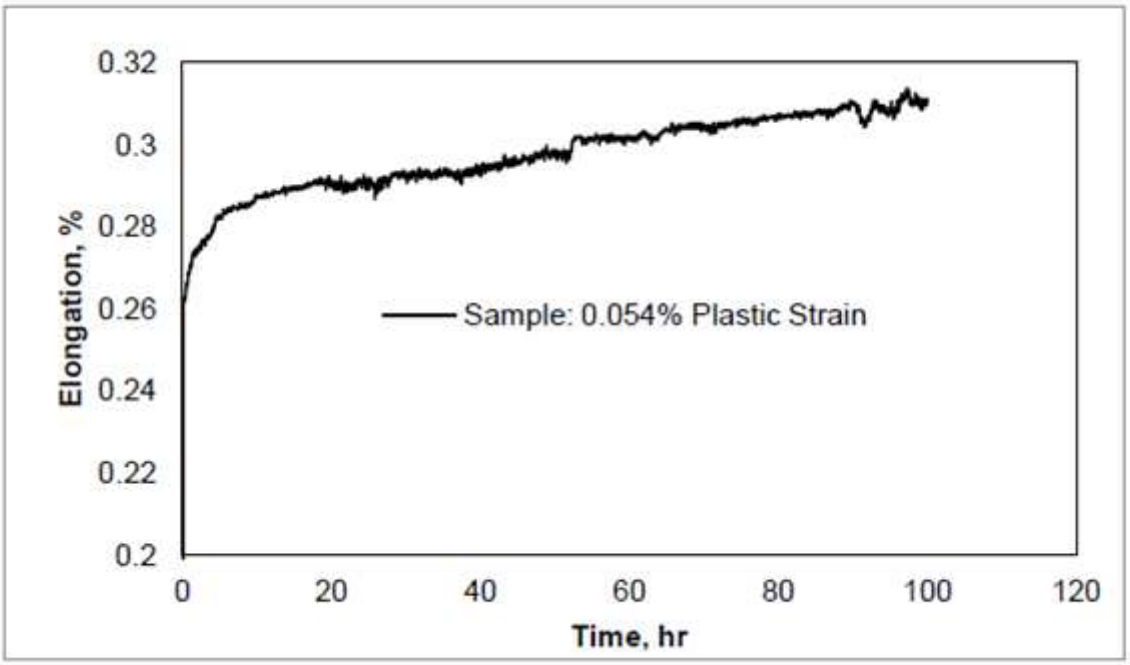

Figure 15

Elongation versus time graph generated during creep testing